Published in final edited form as:
Zhukova, Y., Ulasevich, S. A., Dunlop, J. W. C., Fratzl, P., Möhwald, H., & Skorb, E. V. (2016). Ultrasound-driven titanium modification with formation of titania based nanofoam surfaces. *Ultrasonics Sonochemistry* 36, 146-154. doi:10.1016/j.ultsonch.2016.11.014.

Ultrasound-driven titanium modification with formation of titania based nanofoam surfaces

Abstract

Titanium has been widely used as biomaterial for various medical applications because of its mechanical strength and inertness. This on the other hand makes it difficult to structure it. Nanostructuring can improve its performance for advanced applications such as implantation and lab-on-chip systems. In this study we show that a titania nanofoam on titanium can be formed under high intensity ultrasound (HIUS) treatment in alkaline solution. The physicochemical properties and morphology of the titania nanofoam are investigated in order to find optimal preparation conditions for producing surfaces with high wettability for cell culture studies and drug delivery applications. AFM and contact angle measurements reveal, that surface roughness and wettability of the surfaces depend nonmonotonously on ultrasound intensity and duration of treatment, indicating a competition between HIUS induced roughening and smoothening mechanisms. We finally demonstrate that superhydrophilic bio-and cytocompatible surfaces can be fabricated with short time ultrasonic treatment.

Ultrasound-driven titanium modification with formation of titania based nanofoam surfaces

Yulia Zhukova,* Sviatlana A. Ulasevich, John W. C. Dunlop, Peter Fratzl, Helmuth Möhwald, Ekaterina V. Skorb

Max Planck Institute of Colloids and Interfaces, Am Mühlenberg 1, 14476 Potsdam, Germany

* Corresponding author e-mail: yulia.zhukova@mpikg.mpg.de

Abstract

Titanium has been widely used as biomaterial for various medical applications because of its mechanical strength and inertness. This on the other hand makes it difficult to structure it. Nanostructuring can improve its performance for advanced applications such as implantation and lab-on-chip systems. In this study we show that a titania nanofoam on titanium can be formed under high intensity ultrasound (HIUS) treatment in alkaline solution. The physicochemical properties and morphology of the titania nanofoam are investigated in order to find optimal preparation conditions for producing surfaces with high wettability for cell culture studies and drug delivery applications. AFM and contact angle measurements reveal, that surface roughness and wettability of the surfaces depend nonmonotonously on ultrasound intensity and duration of treatment, indicating a competition between HIUS induced roughening and smoothening mechanisms. We finally demonstrate that superhydrophilic bio- and cytocompatible surfaces can be fabricated with short time ultrasonic treatment.

Keywords: ultrasound, cavitation, titanium, TiO_2, nanotopography, roughness

1. Introduction

Artificial heart valves and joint components, dental implants, orthopedic screws, pacemaker cases, vascular stents are commonly used biomedical applications of titanium-based implants [1]. Titanium is a bioinert metal, it induces a tolerable reaction in the host tissue, shows an adequate resistance to the corrosive *in-vivo* environment, and has the necessary strength, ductility and endurance limit to withstand loading experienced in everyday life [2]. Intense research is still being pursued in the development of new titanium alloys with enhanced biocompatibility and lower elastic modulus closer to bone [3]. Due to its outstanding properties, Ti and its alloys up to nowadays represent the standard in orthopedic

surgery and implantology, in particular, of permanent load-bearing implants [4]. Modifications of the surface at the nanoscale have an effect on the chemical reactivity of a biomedical material affecting biomolecular, ionic and other interactions of the surface with the tissue [6]. Such changes in surface properties, altered by ultrasonic modification, may change wetting properties, leading to different protein adsorption, or influence bone mineralization [5]. Recent advances in regenerative therapies and surface science suggest, that cell adhesion to the implant surface can be regulated by various features of the underlying adhesive substrate, such as its chemical composition, physical properties, and topography (for more information about surface modification strategies and cellular recognition of these surfaces see these review papers [5] [6]). Recent studies in surface nanostructuring suggest that cells respond to nanotopography [7].

The high mechanical strength and inertness of titanium is also the main issue when trying to nanostructure it. Straight-forward known surface treatments of Ti and its alloys (Ti6Al4V)can be divided into three main groups: mechanical, chemical and physical methods [4]. Polishing, machining, blasting belong to the mechanical methods. Chemical manufacturing methods for surface modification are acid- and alkali-treatments, anodic oxidation. Physical methods can be represented by plasma spray treatment [8], ion implantation [9] and laser treatments [10]. These methods can be used either individually or in combination with other treatments, and cause the formation of different nanotopographies with inhomogeneous features. However, the majority of methods for surface nanostructuring are expensive, time consuming, or difficult to apply for large scale implant production [11]. Parameters, which are required for large-scale manufacturing, are the following: 1) ability to simultaneously reach all surfaces in devices with complex geometries (e.g. femoral stems, dental screws and cardiovascular stents); 2) possibility to modify at the nanoscale commercially available biocompatible metals and implants; 3) simple integration into industrial process lines [4]. According to the above mentioned features, chemical treatments seem to be attractive for large-scale manufacturing, because they provide uniform access of the reactive substance to all surfaces, but this leaves often unwanted residuals. In addition chemical treatment needs further processing in the case of annealing of crystalline materials at high temperatures. Thus, it is important to find an alternative technology with minimum chemicals addition for nanoscale modification of titanium, which could be applied for multifaceted devices with complex geometries such as dental screws and cardiovascular stents of potentially partially crystalline materials.

Ultrasound is used in different areas, from surface modification to capsules' opening and diagnostics. High intensity ultrasound (HIUS) is a promising method for the production of nanostructured materials. Ultrasound is a unique energy source [12] which provides energy localization with possible acoustic cavitation phenomena, i.e., the formation, growth, and implosive collapse of cavitation bubbles in a liquid. This collapse is able to produce intense local heating (hot spots with temperatures of roughly 5000 °C) and high pressures of about 500 atm [12]. At the liquid-solid interface, the collapse drives high-speed jets of liquid into the surface, whose impact is sufficient to locally melt most metals [12, 13] and induces significant changes in surface morphology, composition, and reactivity. On contrary to the ultrasound power used for disruption of carriers [14, 15], the ultrasound power used in our study for surface modification is at least 3 times higher.

The strategy we demonstrate here combines the extreme conditions provided for short times by HIUS with a dedicated short term chemical treatment, in special we combine HIUS with an alkali surface treatment. The alkali surface treatment [16] showed an effect analogous to heat treatment on the bone-bonding ability of alkali-treated titanium. Additional treatment with ultrasound [17] can be an attractive method for the production of a partially crystalline titania nanofoam layer strongly adhering to the substrate. It has been used for the development of multifunctional nanomaterials such as bimetallic nanoparticles [18, 19], magnetic nanoparticles [20], nanocomposites [21], mesoporous metal surfaces and sponges [22]. The effect of ultrasound irradiation on the surface morphology and physicochemical properties has been demonstrated in various studies [23, 24]. Metal based surfaces irradiated by HIUS are highly hydrophilic [25] due to their high roughness, and an active oxide layer is formed on the metal surface. The surfaces are porous and attractive as surface encapsulation systems, since no additional surface coating is required for encapsulation of bioactive molecules [26]. High intensity ultrasound (HIUS) offers a fast and versatile methodology for fabrication of nanostructured materials, both inorganic and organic [27], that are often unavailable by conventional methods [28].

This paper contributes to the understanding of the mechanisms involved in titanium surface modification in alkali solution during HIUS. The morphology and chemical properties of the nanostructured surfaces produced by the sonochemical method extensively depend on the various treatment parameters related to HIUS and alkali treatment. HIUS processing is characterized by various ultrasound parameters (amplitude, intensity, frequency), and duration of treatment, which can be summarized as the energy input into the system. Alkali treatment

is characterized by the nature and concentration of the electrolyte solution. In this study, we test the effect of HIUS energy input and alkali treatment on morphology and physicochemical properties of the titanium surface. Furthermore, we investigate the cytocompatibility of the nanostructured titanium surfaces to show prospects of nanostructured materials for bio-application.

2. Experimental Section

Materials

A titanium layer (99.9%) of thickness 400 nm was deposited on glass or silicon substrates by means of Electron Beam Physical Vapor Deposition (EB-PVD). The size of the substrates was (*approx.*) 1 x 1 cm^2 to fit the homemade Teflon sample holder used for HIUS. Prior to sonication, the metal plates were degreased with isopropanol and rinsed with Milli-Q water (18 MΩ·cm).

Bulk titanium or its alloys, although being very tough, can be used for modification. In our experiments with cell studies it is advantageous to use a nanoscale-thick Ti layer on a glass substrate rather than bulk titanium, since the optical observation of the cell growth requires transparent samples. The formed titania nanofoam layer on glass is transparent enough to observe cell adhesion and growth on the surface. Closest to bulk titanium are thicker layers, 400 nm to 150 nm. Thus, as model we use a 400 nm deposited layer on glass or on silicon for atomic force microscopy study.

Fabrication of nanostructured surfaces

Samples were ultrasonically treated in presence of sodium hydroxide using the ultrasonic processor UIP1000hd (Hielscher Ultrasonics GmbH, Germany) with a maximum output power of 1000 W. The apparatus was equipped with a sonotrode BS2d18 (head area 2.5 cm^2) and a booster B2-2.2, magnifying the working amplitude 2.2 times. Sonication parameters are controlled and presented in Fig. 1. Sonication was performed at *ca*. 20 kHz and constant temperature of around 333 K monitored by the thermo sensor inserted into the working solution. In order to investigate the effect of preparation conditions on the morphology of nanostructured titanium surfaces, samples were treated with ultrasound of different amplitude (60, 70, 80%) for different time periods (3, 5, 7, 10, and 15 minutes). The

maximum intensity was calculated to be 250 W cm^{-2} at mechanical amplitude of 187 µm (at 100%). After treatment the samples were additionally rinsed with isopropanol and water.

The calculation of the energy corresponding to each ultrasonic intensity and duration of treatment is given below. Firstly, according to operating instructions for UIP1000hdT, the maximal mechanical amplitude at 100 % for the sonotrode BS2d18 without booster is 85 µm. With an enhancing booster B2-2.2, the maximal mechanical amplitude was increased by a factor of 2.2 and A_{100}=187 µm, which correspond to the maximal ultrasonic intensity I_{100}=250 W cm^{-2}. The equipment was operated at three amplitudes 80, 70 and 60 %, which correspond to ultrasonic intensities I_1=200, I_2=175 and I_3=150 W cm^{-2}. The total power output of an ultrasonic unit is the product of the sonotrode frontal area S and ultrasonic intensity (Eqs. 1).

$$P[W] = I\left[Wcm^{-2}\right] \times S\left[cm^2\right] \quad (1)$$

The energy E is the product of the corresponding power output P and the time of exposure t:

$$E[Ws] = P[W] \times t[s] \quad (2)$$

After rearranging, Equ. 2 becomes:

$$E[Ws] = I\left[Wcm^{-2}\right] \times S\left[cm^2\right] \times t[s] \quad (3)$$

The values of energy corresponding to ultrasonic intensities and durations of treatment are given in Table 1.

Atomic Force Microscopy (AFM)

AFM measurements were carried out in air at room temperature in tapping mode with micro cantilevers OMCL-AC160TS-W (Olympus, Japan). Typical cantilever values: resonance frequency 300 kHz; spring constant 42 N/m. Atomic force micrographs of a scan size 3 x 3 μm^2 were made on three different places on the sample. Image analysis was carried out with the software Nanoscope V614r1. Quantitative data about the surface roughness, height profile, and three-dimensional projections of the micrographs were obtained using this software. The surface roughness was quantified by the software as an arithmetic average of the absolute values of the surface height deviations measured from the mean plane:

$$R_a = \frac{1}{N}\sum_{j=1}^{N}\left|Z_j\right| \quad (4)$$

Water contact angle measurements

The contact angle was measured using the homemade system described in ref. [29]. Measurements were performed with a 1 µl water droplet deposited onto the titanium substrates with a syringe from the top. During the process, the contact angles, from the left θ_L and from the right θ_R, are continuously monitored. After that, the average contact angles $\overline{\theta_L}$ and $\overline{\theta_R}$, $\Delta\theta$ and an average contact angle $\overline{\theta}$ were calculated as follows:

$$\left|\overline{\theta_R} - \overline{\theta_L}\right| = \Delta\theta \tag{5}$$

$$\frac{\overline{\theta_R}}{2} + \frac{\overline{\theta_L}}{2} = \overline{\theta} \tag{6}$$

Untreated titanium substrates were used as a control.

Scanning Electron Microscopy (SEM)

Prior to microscopy the samples were sputtered with gold. SEM was conducted with a Gemini Leo 1550 instrument (Leo Elektronenmikroskopie GmbH, Germany) at an operating voltage of 3 keV.

Transmission Electron (High-resolution) Microscopy (TEM, HRTEM)

Transmission electron microscopy (TEM) measurements were performed on a Zeiss EM 912 Omega (Carl Zeiss AG, Germany) transmission electron microscope operated at 300 kV and equipped with an electron-diffraction (ED) unit. High-resolution transmission electron microscopy (HRTEM) was performed by TEM in a Philips CM30 operated at 300 kV. The samples were ultramicrotomed (Leica EM FC6) and placed onto carbon-coated copper grids.

Cell culture studies

A mouse calvarial preosteoblast cell line MC3T3-E1 was obtained from the Ludwig Boltzmann Institute, Vienna, Austria. Preosteoblasts were cultured in α-MEM supplemented with 10 % (by volume) fetal calf serum (FCS), 4500 mg glucose, 0.1 % (by volume) gentamycin, 0.1 % (by volume) ascorbic acid, and maintained at 37 °C with 5 % CO_2 in humidified atmosphere. Cells were passaged in total three times every 24 hours by a dilution factor of 1/6. After reaching confluence, cells were removed from the culture vessels by incubating with pronase for 3 – 5 min and seeded onto glass and TMS surfaces at

6000 cells/cm^2. Three samples were tested per substrate type, three independent experiments were conducted. All surfaces and scaffolds were autoclaved before cell culture experiments. After 3 hours of growth optical images were obtained with a phase contrast microscope.

Actin cytoskeleton staining

The surfaces were washed with phosphate buffer saline (PBS), fixed with 4% paraformaldehyde in PBS, and permeabilized with buffered Triton-X100 (Sigma-Aldrich, Steinheim, Germany) for 10 min at room temperature. The scaffolds were then thoroughly washed with PBS and stained for 60-90 min with phalloidin Alexa488 (Invitrogen, Oregon, USA) (1:20) in dark at 4°C. After that scaffolds were thoroughly washed with PBS again, and stained for nuclei with TO-PRO3 iodide (Invitrogen, Oregon, USA) (1:300) for 5 min at room temperature. The scaffolds were washed with PBS, mounted with Fluoro-Mount in inverted position on the glass slides, and examined via confocal microscopy (Leica Microsystems, Mannheim, Germany).

3. Results and Discussion

In this study, we test first the effect of processing parameters, such as HIUS energy input and alkali treatment, on morphology and physicochemical properties of the titanium surface, then the cytocompatibility of the nanostructured surfaces. The focus is on formation of a nanofoam layer. In water Ti exhibits minor nanofoam layer formation after 60 min of sonication [30]. Ti has a high melting point, and the physical effect of melting is prevalent over other effects of ultrasonic irradiation, therefore one can observe a slight increase in surface roughness. However, by additional treatment in NaOH one can enhance the chemical effects of ultrasonic treatment.

The HIUS treatment gives rise to four different morphological stages (Figure 2), starting with an untreated flat titanium (Fig. 2, untreated sample). It has a native oxide layer mainly composed of the stable oxide TiO_2 and is typically 3-7 nm thick [31]. Flat titanium is treated with HIUS in presence of an aqueous solution of NaOH. In the early stage of HIUS treatment in NaOH solution, a native titanium oxide layer is removed, mainly mechanically disrupted by HIUS and a mesoporous titanium dioxide layer is being formed on the exposed surface (Fig. 2, stage I). With further alkali treatment more hydroxyls attack hydrated TiO_2, leading to negatively charged hydrates on the metal surface:

$$TiO_2 \cdot nH_2O + OH^- \leftrightarrow HTiO_3^- \cdot nH_2O \quad (7)$$

The growth of titanate nanobelts perpendicularly from the titanium scaffold is displayed in Fig. 2, Stage II, and finally, the formation of a complex hierarchical structure takes place (Fig. 2, Stage III). For biological applications mesoporous titanium with the pronounced nanofoam layers was used. In previous work on aluminium alloys [32], the strongest adhesion was observed before the layer formed at Stage I. Moreover, together with the strongest adhesion, the layer formed after Stage I covered the surface uniformly. This will be discussed further being the most promising as novel strategy for titanium implant treatment.

What are the effects of high intensity ultrasonic treatment one can use to overcome a TiO_2 layer? The titanium covered with a native layer (Ti/TiO_2) is shown in Figure 3a. Due to physical impact, bubble collapse with high energy jets, the oxide layer is expected to break [12]. The sonochemical etching during treatment in alkali medium is obvious. The early study of Ziemniak *et al* [33] showed the solubility behavior of TiO_2 in alkali media, e.g. in aqueous sodium hydroxide. The main oxidation state is Ti^{4+}, although due to sonochemical non-equilibrium conditions one can expect also the states Ti^{3+} and Ti^{2+}, that are less stable, as intermediate resulting in an advanced nanostructured surface with an interesting morphology for cell growth studies. In basic solution the negative charge on the titanium surface increases with increasing pH [31]. It was shown [27, 28], that during the hydrothermal alkali treatment the passive protective TiO_2 layer partially dissolves into alkaline solution because of the impact of the hydroxyl groups:

$$TiO_2 + OH^- \rightarrow HTiO_3^- \quad (8)$$

In our study, the native oxide layer breaks up due to the physical effect of HIUS and, contrary to the hydrothermal treatment, results in interplay between reactions with TiO_2 and Ti with formation of an interpenetrating “domain-like” layer of complex structure (Figure 3b). The reaction proceeds simultaneously with the hydration of TiO_2 (Eq. 8) and Ti :

$$Ti + 3OH^- \rightarrow Ti(OH)_3^+ + 4e^- \quad (9)$$

$$Ti(OH)_3^+ + e^- \rightarrow TiO_2 \cdot H_2O + 0.5H_2 \uparrow \quad (10)$$

$$Ti(OH)_3^+ + 3H_2 \rightarrow Ti^0 + 3H_2O + 3H^+ \quad (11)$$

$$Ti(OH)_3^+ + OH^- \leftrightarrow Ti(OH)_4 \quad (12)$$

High-intensity ultrasound induces a wide range of chemical and physical consequences. The chemical effects of ultrasound derive primarily from acoustic cavitation. The extreme temperatures and pressures induce sonolysis and generation of highly reactive radicals [12], which chemically transforms the solid surface. This allows acceleration of a chemical reaction at the solid-liquid interface, reactivity enhancement of the solids, and permits use of less aggressive chemicals. The physical effects include (1) improvement of mass transport from local turbulent flow and microstreaming, (2) generation of surface erosion and pitting at liquid-solid interfaces by shock waves and microjets, (3) generation of high-velocity interparticle collisions in liquid-solid slurries, and (4) fragmentation of fragile solids to increase the surface area [27]. The combination of physical and chemical effects allows a one-step straight forward modification of metal surfaces.

Thus, the final structure, shown in Figure 3c, should be hydrophilic due to surface –OH groups. In contrast to surfaces experiencing hydrothermal treatments, the layer of formed oxidized structure can be partially crystalline due to the high energy of the HIUS applied to the system and extreme heating/cooling rates known for the process. The low magnification TEM image of the cross section of the film-substrate interface points to adhesion of the formed interpenetration layer to titanium (Fig. 4a). The HRTEM and ED micrographs detected the TiO_2 (004) peak which correspond to anatase (Fig. 4b). This experimental observation correlates to the hydration of Ti in alkali solution (Eq. 10).

The intensity and duration of ultrasound treatment significantly affect the formation of a mesoporous titania surface. At ultrasound intensities 150 – 200 W cm^{-2} formation of a "domain-like" structure starts to form due to the development of the TiO_2 layer. Maturation mainly develops with the increase of duration and intensity of ultrasonication (Fig. 5). Surface roughness R_a and contact angle of three points on the surface are plotted *vs*. time (Fig. 5 a, c) and *vs*. energy (Fig. 5 b, d) for different ultrasound intensities (Fig. 6). For all intensities one observes a non-monotonous behavior of roughness development with duration of HIUS treatment. The highest surface roughness 15±2 nm could be achieved at highest I_2 and 10 min of treatment. Quite high surface roughness was achieved for I_1 at 5 and 10 min of treatment, 14±2 nm, respectively. For all three US intensities, one can observe the following dependence: after the first peak with the high surface roughness is achieved, the roughness first drops, but after some time it increases again, reaching the highest value of the first peak. One observes the same cyclic dependence for all three intensities; however, the peak positions vary. For instance, the curves I_1 and I_3 have analogous shapes with similar peak positions;

however curve I_1 looks smoother than I_2, which corresponds to smaller changes in surface roughness. The surface roughness does not monotonously increase but one observes its oscillations on the nanoscale. Two possible reasons for such oscillatory behavior can be assumed. The first one is based on purely mechanical effects, i.e. on two opposing forces: mechanical surface disruption increasing roughness and flaking off reducing the roughness. For instance, at high US intensities one can achieve high roughness at already 5 min of sonication. With further treatment, a strongly modified layer is flaking off and gets flatter, therefore, the drop in surface roughness. After that, the surface is modified again, and the roughness increases. The second explanation is based on a more complex effect, an interplay between the number of bubble collapse events and temperature effect [34] of the HIUS. The more bubble collapses takes place, the higher the roughness increases, however due to the corresponding temperature increase, the surface smoothens again. This cycle repeats. Although we use the additional NaOH treatment in order to accelerate chemical effects of HIUS over the physical ones, a local temperature variation still seems to have an impact on surface roughness, which appears as nanoscale roughness oscillations. The second explanation seems more probable, because during the flaking off one will probably obtain stronger drops and less periodic oscillations of surface roughness. We used 5M NaOH aqueous solution with pH 13. At lower alkali concentrations pH 9 and 11, modification takes place, but at the same HIUS conditions does not provide surface roughening higher than 10 nm.

The water contact angle measurements provide evidence, that the HIUS-modified titanium surfaces exhibit extremely high hydrophilicity (θ below 10°), which may be called superhydrophilic [35]. In order to measure very low contact angles, we used a homemade system [29], where the contact angles, from the left θ_L and from the right θ_R, are continuously monitored (Fig. 7). The differences may be due to impurities and inhomogeneities of the surface chemistry and morphology. The lowest contact angle value θ = 3.3 ± 1.6° corresponds to the peak with the highest surface roughness (I_1=200 W cm^{-2}), and this holds for all three US intensities. After that, contact angle values rise and drop again, reaching the first low value. Here, the curve I_3 shows the most significant fluctuations in contact angle with energy input, however, the contact angle values are still higher than for the higher intensities. Thus, contact angle changes depend on time and energy input nonmonotonously, similar to the oscillating behavior of surface roughness (Fig. 6 c, d). In addition, similar behavior was demonstrated for the changes of water droplet size in time for

different US intensities (fig. 6 e, f). The following observations of water droplet size are in good agreement with changes of contact angle: (1) the fluctuations of droplet size are reversely dependent on contact angle value for all three US intensities: large water droplets correspond to small contact angles; (2) the biggest droplet size corresponds to the lowest contact angle value $\theta = 3.3 \pm 1.6°$ at I_I=200 W cm^{-2}; (3) It is known, that the contact angle is sensitive to local geometrical transformations of the solid surface. The superhydrophilicity of the surface may be due to the nanosize features on the surface: an intrinsically hydrophobic surface becomes more hydrophobic [36], as its roughness increases, and the hydrophilicity increases with roughness for the intrinsically hydrophilic surface [37]. In our case, we deal with the intrinsically hydrophilic Ti surface due to the native TiO_2. The surface roughness of TMS surfaces does not increase continuously but changes in an oscillatory manner. The contact angle changes accordingly with nonmonotonic behavior of surface roughness. It becomes more hydrophilic with increase of surface roughness.

Nanostructured titanium has to perform well across two interfaces: between the bulk metal and the interpenetrating layer, and between the interpenetrating layer and the tissue (Fig. 8). Investigation of the physicochemical properties of the mesoporous titanium surface has demonstrated the unique achievement by HIUS treatment in NaOH. Due to its continuous transition from surface to bulk, the interpenetrating TiO_2 layer has high bonding strength to the bulk metal (Fig. 8 a). In order to estimate the cytocompatibility of the produced TMS surfaces, cell culture studies with a MC3T3-E1 preosteoblast cell line were performed. Different stages of tissue formation were investigated: early stages at 24h, 48h, and 5 days of cell incubation on the TMS surfaces. The cell behavior was examined by confocal microscopy. At early stages (Fig. 8 b), we observed quite large single cells with an easily identified nucleus, which start to spread and to form cell-cell contacts. At higher levels of proliferation (Fig. 8 c), the cells form numerous cell-cell contacts, and complete coverage of the TMS surface is achieved. For the investigation of tissue growth for longer times, cells were seeded onto the tissue engineering scaffolds with round channels of 500 µm diameter treated with HIUS. The cells formed 50-70 µm thick tissue within the microchannels after 5 days of incubation (Fig. 8 d), and the kinetics of tissue growth could be quantified by measuring the projected tissue area in the microchannel (Fig. 8 e) as described in [38, 39]. The amount of tissue formed in the channels modified with HIUS was found to be larger than in unmodified ones. This observation demonstrates an important effect of nanostructuring on tissue growthand demostrates that TMS can firmly integrate with the preosteoblast cell line MC3T3-E1 at different time points of tissue growth. Our results suggest that the titanium

nanotopography can have a significant effect both on individual cells and tissue. The behavior of the first cell layer is important to understand and control, since we believe it to play a crucial role in the further tissue formation. As such this will be an important focus of further cell culture studies on TMS surfaces. Much research has been done on understanding 3D tissue growth in channels of different geometries. It has been shown that after cells completely cover the substrate, tissue growth, at later time points than those studied here, could be described by a model for curvature-controlled growth. This suggests that by tuning the geometry of the scaffolds for tissue engineering at multiple length scales it is not only possible to accelerate growth by large scale geometries [35], but also by controlling nano-scale topographies as demonstrated here. Further studies are needed to investigate this in more detail.

4. Conclusions

This work contributes to the fundamental understanding of the mechanism of acoustic cavitation at the titanium surface in combination with alkali treatment. We have shown an elaborated multistage process of titanium surface nanostructuring with HIUS in NaOH. By controlling the treatment parameters such as ultrasound intensity and duration of treatment, control over physical, chemical, and structural properties of the titanium surface is achieved. Conditions optimal for the formation of nanostructured TMS were found via SEM, TEM, AFM, and contact angle measurements. Sonication in alkali conditions induces changes of surface nanotopography, wettability and crystallinity of the titania surfaces. Due to the interplay between physical and chemical effects of the proposed technique, short HIUS treatment is sufficient for formation of a nanostructured titanium dioxide surface. This surface presents good cytocompatibility for MC3T3-E1 preosteoblasts, which makes them suitable for biological applications.

Acknowledgements

We gratefully acknowledge the assistance from Anneliese Heilig in AFM measurements, Rona Pitschke and Heike Runge for performing SEM, and Christine Pilz-Allen in assistance with cell culture maintenance. We thank Dr. Daria V. Andreeva, PC II Bayreuth University, for the help with organization of vacuum deposition of titanium layers

on different substrates to have a model system with initial precise roughness. We thank Olga Baidukova for assistance with CLSM.

References

[1] F. Variola, J.B. Brunski, G. Orsini, P. Tambasco de Oliveira, R. Wazen, A. Nanci, Nanoscale surface modifications of medically relevant metals: state-of-the art and perspectives, Nanoscale 3 (2011) 335-353.

[2] T. Albrektsson, P.I. Branemark, H.A. Hansson, J. Lindstrom, Osseointegrated titanium implants - requirements for ensuring a long-lasting, direct bone-to-implant anchorage in man, Acta Orthopaedica Scandinavica 52 (1981) 155-170.

[3] M. Geetha, A.K. Singh, R. Asokamani, A.K. Gogia, Ti based biomaterials, the ultimate choice for orthopaedic implants – A review, Prog. Mater Sci. 54 (2009) 397-425.

[4] F. Variola, J. Brunski, G. Orsini, P.T. de Oliveira, R. Wazen, A. Nanci, Nanoscale surface modifications of medically-relevant metals: state-of-the art and perspectives, Nanoscale 3 (2011) 335-353.

[5] S. Bauer, P. Schmuki, K. von der Mark, J. Park, Engineering biocompatible implant surfaces: Part I: Materials and surfaces, Prog. Mater Sci. 58 (2013) 261-326.

[6] K. von der Mark, J. Park, Engineering biocompatible implant surfaces: Part II: Cellular recognition of biomaterial surfaces: Lessons from cell–matrix interactions, Prog. Mater Sci. 58 (2013) 327-381.

[7] C. Selhuber-Unkel, T. Erdmann, M. López-García, H. Kessler, U.S. Schwarz, J.P. Spatz, Cell Adhesion Strength Is Controlled by Intermolecular Spacing of Adhesion Receptors, Biophys. J. 98 (2010) 543-551.

[8] B.S. Necula, I. Apachitei, L.E. Fratila-Apachitei, E.J. van Langelaan, J. Duszczyk, Titanium bone implants with superimposed micro/nano-scale porosity and antibacterial capability, Appl. Surf. Sci. 273 (2013) 310-314.

[9] S. Ferraris, A. Venturello, M. Miola, A. Cochis, L. Rimondini, S. Spriano, Antibacterial and bioactive nanostructured titanium surfaces for bone integration, Appl. Surf. Sci. 311 (2014) 279-291.

[10] V. Dumas, A. Rattner, L. Vico, E. Audouard, J.C. Dumas, P. Naisson, P. Bertrand, Multiscale grooved titanium processed with femtosecond laser influences mesenchymal stem cell morphology, adhesion, and matrix organization, J. Biomed. Mater. Res., Part A 100A (2012) 3108-3116.

[11] J. Banhart, Manufacture, characterisation and application of cellular metals and metal foams, Prog. Mater Sci. 46 (2001) 559-632.

[12] K.S. Suslick, Sonochemistry, Science 247 (1990) 1439-1445.

[13] S. Doktycz, K. Suslick, Interparticle collisions driven by ultrasound, Science 247 (1990) 1067-1069.

[14] B.G. De Geest, A.G. Skirtach, A.A. Mamedov, A.A. Antipov, N.A. Kotov, S.C. De Smedt, G.B. Sukhorukov, Ultrasound-Triggered Release from Multilayered Capsules, Small 3 (2007) 804-808.

[15] A.G. Skirtach, B.G. De Geest, A. Mamedov, A.A. Antipov, N.A. Kotov, G.B. Sukhorukov, Ultrasound stimulated release and catalysis using polyelectrolyte multilayer capsules, J. Mater. Chem. 17 (2007) 1050-1054.

[16] S. Nishiguchi, T. Nakamura, M. Kobayashi, H.-M. Kim, F. Miyaji, T. Kokubo, The effect of heat treatment on bone-bonding ability of alkali-treated titanium, Biomaterials 20 (1999) 491-500.

[17] E.V. Skorb, D.V. Andreeva, H. Möhwald, Generation of a Porous Luminescent Structure Through Ultrasonically Induced Pathways of Silicon Modification, Angew. Chem. Int. Ed. 51 (2012) 5138-5142.

[18] J. Dulle, S. Nemeth, E.V. Skorb, T. Irrgang, J. Senker, R. Kempe, A. Fery, D.V. Andreeva, Sonochemical Activation of Al/Ni Hydrogenation Catalyst, Adv. Funct. Mater. 22 (2012) 3128-3135.

[19] P.V. Cherepanov, I. Melnyk, E.V. Skorb, P. Fratzl, E. Zolotoyabko, N. Dubrovinskaia, L. Dubrovinsky, Y.S. Avadhut, J. Senker, L. Leppert, S. Kummel, D.V. Andreeva, The use of ultrasonic cavitation for near-surface structuring of robust and low-cost AlNi catalysts for hydrogen production, Green Chem. 17 (2015) 2745-2749.

[20] O. Baidukova, H. Mohwald, A.S. Mazheika, D.V. Sviridov, T. Palamarciuc, B. Weber, P.V. Cherepanov, D.V. Andreeva, E.V. Skorb, Sonogenerated metal-hydrogen sponges for reactive hard templating, Chem. Commun. 51 (2015) 7606-7609.

[21] E.V. Skorb, O. Baidukova, A. Goyal, A. Brotchie, D.V. Andreeva, H. Mohwald, Sononanoengineered magnesium-polypyrrole hybrid capsules with synergetic trigger release, J. Mater. Chem. 22 (2012) 13841-13848.

[22] Cavitation: A novel energy-efficient technique for the generation of nanomaterials, Taylor & Francis group, LLC, 2014.

[23] M. Virot, T. Chave, S.I. Nikitenko, D.G. Shchukin, T. Zemb, H. Möhwald, Acoustic Cavitation at the Water–Glass Interface, The Journal of Physical Chemistry C 114 (2010) 13083-13091.

[24] M. Virot, R. Pflieger, E.V. Skorb, J. Ravaux, T. Zemb, H. Möhwald, Crystalline Silicon under Acoustic Cavitation: From Mechanoluminescence to Amorphization, J. Phys. Chem. C 116 (2012) 15493-15499.

[25] E.V. Skorb, H. Mohwald, 25th anniversary article: Dynamic interfaces for responsive encapsulation systems, Adv. Mater. 25 (2013) 5029-5043.

[26] D.V. Andreeva, D.V. Sviridov, A. Masic, H. Möhwald, E.V. Skorb, Nanoengineered Metal Surface Capsules: Construction of a Metal-Protection System, Small 8 (2012) 820-825.

[27] K.S. Suslick, G.J. Price, Applications of ultrasound to materials chemistry, Annu. Rev. Mater. Sci. 29 (1999) 295-326.

[28] J.H. Bang, K.S. Suslick, Applications of Ultrasound to the Synthesis of Nanostructured Materials, Adv. Mater. 22 (2010) 1039-1059.

[29] S. Karpitschka, H. Riegler, Quantitative Experimental Study on the Transition between Fast and Delayed Coalescence of Sessile Droplets with Different but Completely Miscible Liquids, Langmuir 26 (2010) 11823-11829.

[30] E.V. Skorb, D. Fix, D.G. Shchukin, H. Mohwald, D.V. Sviridov, R. Mousa, N. Wanderka, J. Schaferhans, N. Pazos-Perez, A. Fery, D.V. Andreeva, Sonochemical formation of metal sponges, Nanoscale 3 (2011) 985-993.

[31] X. Liu, P. Chu, C. Ding, Surface modification of titanium, titanium alloys, and related materials for biomedical applications, Mater. Sci. Eng., R 47 (2004) 49-121.

[32] E.V. Skorb, D.G. Shchukin, H. Mohwald, D.V. Andreeva, Ultrasound-driven design of metal surface nanofoams, Nanoscale 2 (2010) 722-727.

[33] S.E. Ziemniak, M.E. Jones, K.E.S. Combs, Solubility behavior of titanium(IV) oxide in alkaline media at elevated temperatures, J. Solution Chem. 22 601-623.

[34] P.V. Cherepanov, A. Kollath, D.V. Andreeva, Up to which temperature ultrasound can heat the particle?, Ultrason. Sonochem. 26 (2015) 9-14.

[35] J. Drelich, E. Chibowski, D.D. Meng, K. Terpilowski, Hydrophilic and superhydrophilic surfaces and materials, Soft Matter 7 (2011) 9804-9828.

[36] A.B.D. Cassie, S. Baxter, Wettability of porous surfaces, Trans. Faraday Soc. 40 (1944) 546-551.

[37] R.N. Wenzel, Resistance of solid surfaces to wetting by water, Ind. Eng. Chem. 28 (1936) 988-994.

[38] C.M. Bidan, K.P. Kommareddy, M. Rumpler, P. Kollmannsberger, Y.J.M. Bréchet, P. Fratzl, J.W.C. Dunlop, How Linear Tension Converts to Curvature: Geometric Control of Bone Tissue Growth, PLoS ONE 7 (2012) e36336.

[39] C.M. Bidan, K.P. Kommareddy, M. Rumpler, P. Kollmannsberger, P. Fratzl, J.W.C. Dunlop, Geometry as a Factor for Tissue Growth: Towards Shape Optimization of Tissue Engineering Scaffolds, Adv. Healthcare Mater. 2 (2013) 186-194.

Figure 1. A) Experimental setup; B) Homemade Teflon sample holder; C) Ultrasonic processor UIP1000hd (Hielscher Ultrasonics GmbH, Germany) equipped with a sonotrode BS2d18 and booster B2-2.2. Sonotrode BS2d18: diameter 18 mm, approx. length 125 mm; booster B2-2.2: booster B2-2.2: diameter 70 mm, approx. length 115 mm.

Figure 2. Schematic diagram of the morphological stages of the HIUS-alkali treated titanium surface: untreated flat titanium (Untreated Sample); mesoporous titanium dioxide layer formed during the HIUS treatment in NaOH solution (Stage I); titanate nanobelts (Stage II) and hierarchical porous titania (Stage III) formed with further alkali treatment. Surface nanotopographies were observed by SEM.

Figure 3. Schematic illustration of the structuring process taking place during the HIUS treatment of a titanium surface in aqueous solution of NaOH.

Figure 4. a) TEM images of areas of an interpenetration layer of amorphous titania well adhering to titanium with inclusions of b) shown in HRTEM and electron diffraction (ED) crystalline TiO_2.

Figure 5. AFM micrographs and 3D projections of the ultrasonically modified titanium surface at different intensities and duration: 15 min at intensity 150 W cm^{-2} (a); 15 min at intensity 200 W cm^{-2} (b); 3 min at intensity 150 W cm^{-2} (c); 3 min at intensity 200 W cm^{-2} (d). Scale bar is 1 µm.

Figure 6. Oscillations of surface roughness R_a (a, b), contact angle (c, d), and water droplet size (e, f) as a function of sonication time and energy at three ultrasound intensities: I_1=200, I_2=175, and I_3=150 W cm^{-2}. (*) Measurement is done for 10 samples.

Figure 7. Contact angle measurements. The contact angles, from the left θ_L and from the right θ_R, are continuously monitored. For the calculations, only the parallel horizontal regions were taken into account.

Figure 8. Nanostructured titanium has to perform well across two interfaces: between the bulk metal and the interpenetrating layer, and between the interpenetrating layer and the tissue (a). Colors of circles correspond to the same materials as in Figure 3. Due to its unique properties achieved with HIUS treatment in NaOH, the mesoporous titanium surface has high bonding strength to the bulk metal. It can firmly integrate with the preosteoblast cell line MC3T3-E1 at different stages of tissue formation: individual cells after 24h of growth (b), cell layers after 48h (c), and tissue growth in tissue engineering scaffolds after 5 days (d).

Confocal microscopy images with nuclear (red) and actin (green) staining. Scale bar is 100 µm. Quantitative analysis of tissue growth in circular pores of 500 µm diameter unmodified (initial) and modified with HIUS (e).

Energy, [W s]			
Exposure time, [min]	Ultrasonic intensity, [W cm^{-2}]		
	150 (at 60%)	175 (at 70%)	200 (at 80%)
3	27000	31500	36000
5	45000	52500	60000
7	63000	73500	84000
10	90000	105000	120000
15	135000	157500	180000

Table 1. Energy of sonication used at different amplitudes and exposure times.

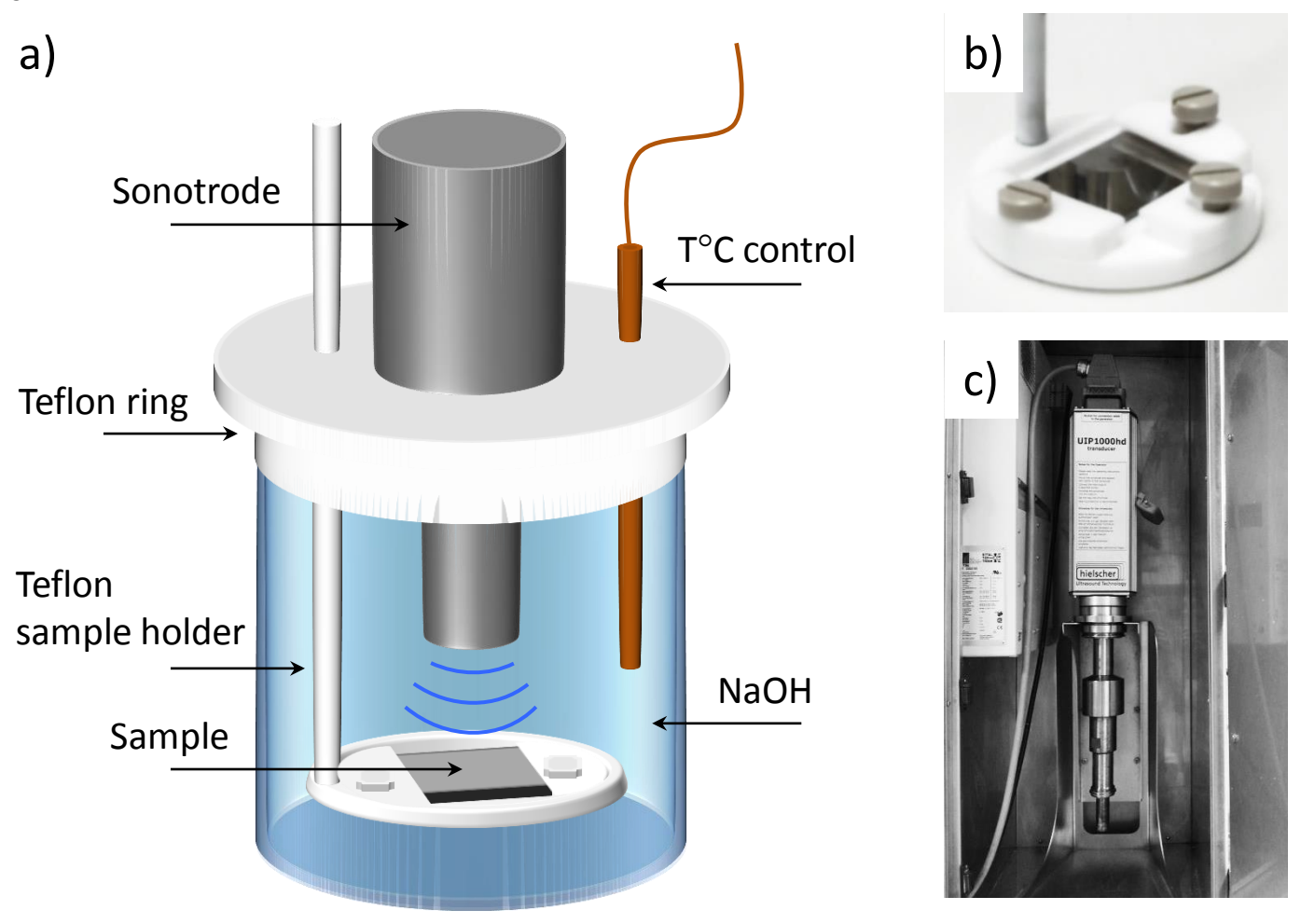
a)
Sonotrode
T°C control
Teflon ring
Teflon
sample holder
Sample
NaOH
b)
c)
UIP1000hd
transducer
hielscher
Ultrasound Technology

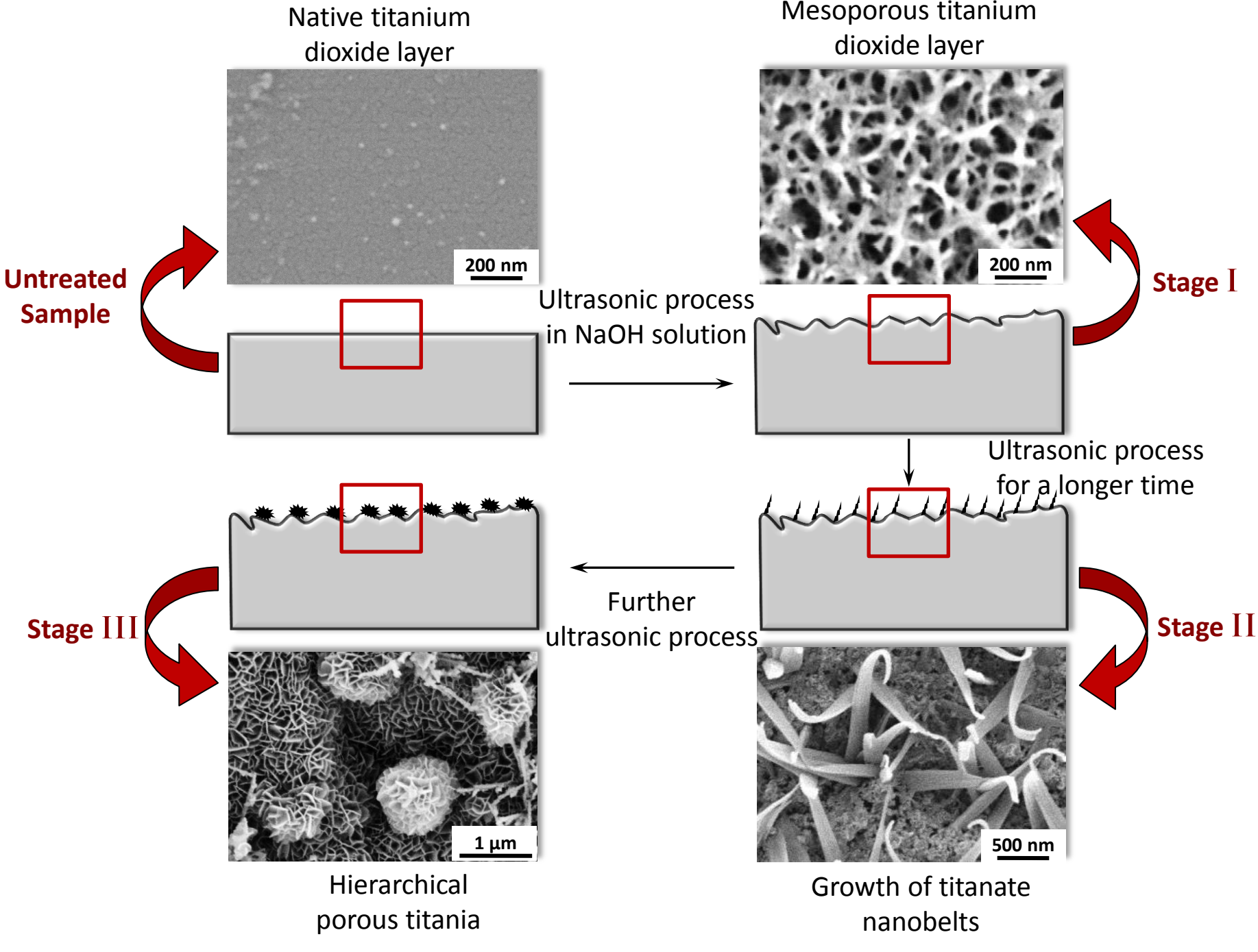
Native titanium dioxide layer
200 nm
Mesoporous titanium dioxide layer
200 nm
Untreated Sample
Stage I
Ultrasonic process in NaOH solution
Ultrasonic process for a longer time
Stage III
Further ultrasonic process
Stage II
1 µm
500 nm
Hierarchical porous titania
Growth of titanate nanobelts

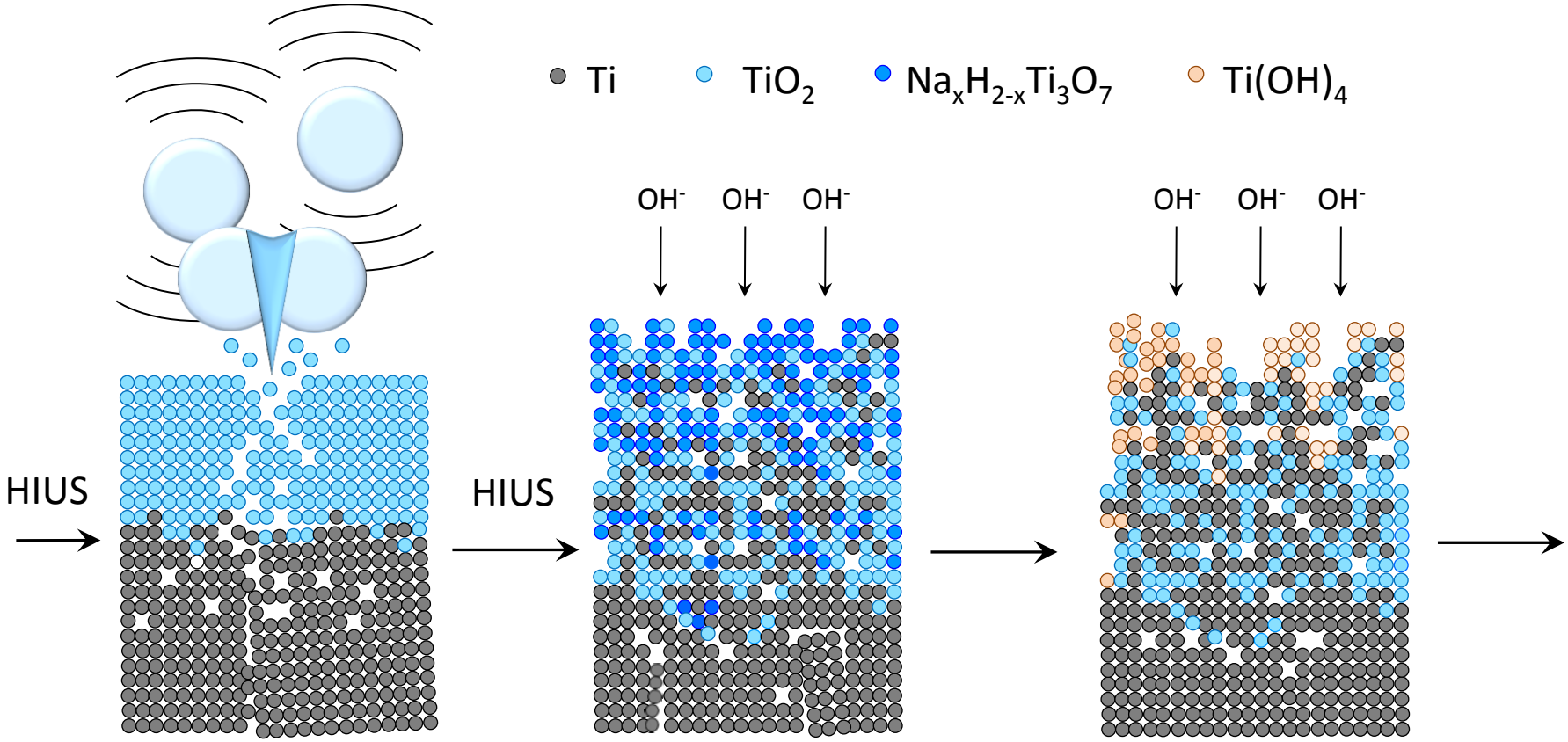

Disruption of native oxide layer with HIUS

$$TiO_2 + OH^- \rightarrow HTiO_3^-$$

$$Ti + 3OH^- \rightarrow Ti(OH)_3^+ + 4e^-$$

$$Ti(OH)_3^+ + e^- \rightarrow TiO_2H_2O + 0.5H_2^0 \uparrow$$

$$Ti(OH)_3^+ + H_2^0 \leftrightarrow Ti^0 + 3H_2O + 3H^+$$

$$Ti(OH)_3^+ + OH^- \leftrightarrow Ti(OH)_4$$

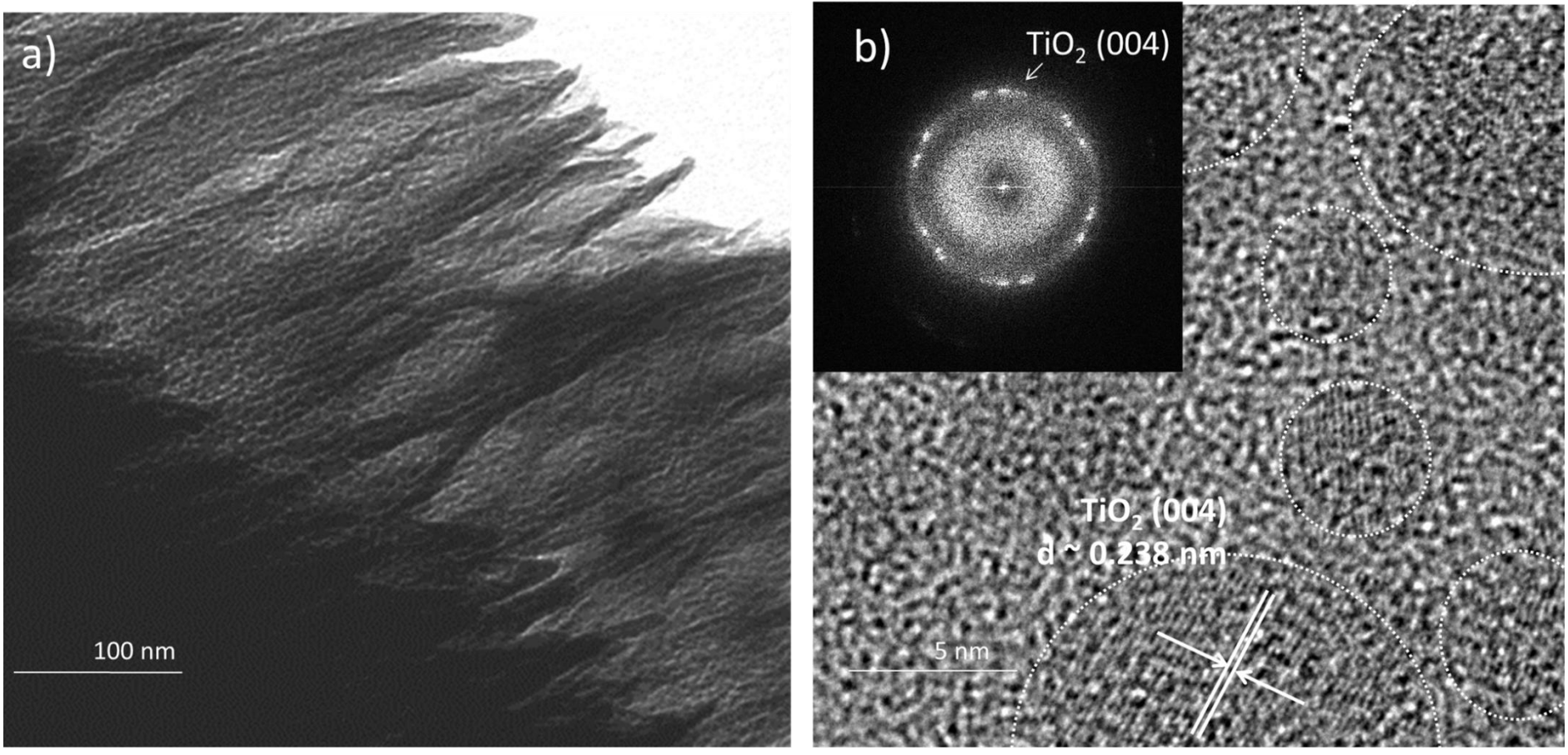
a)
100 nm
b)
TiO2 (004)
TiO2 (004)
d ~ 0.238 nm
5 nm

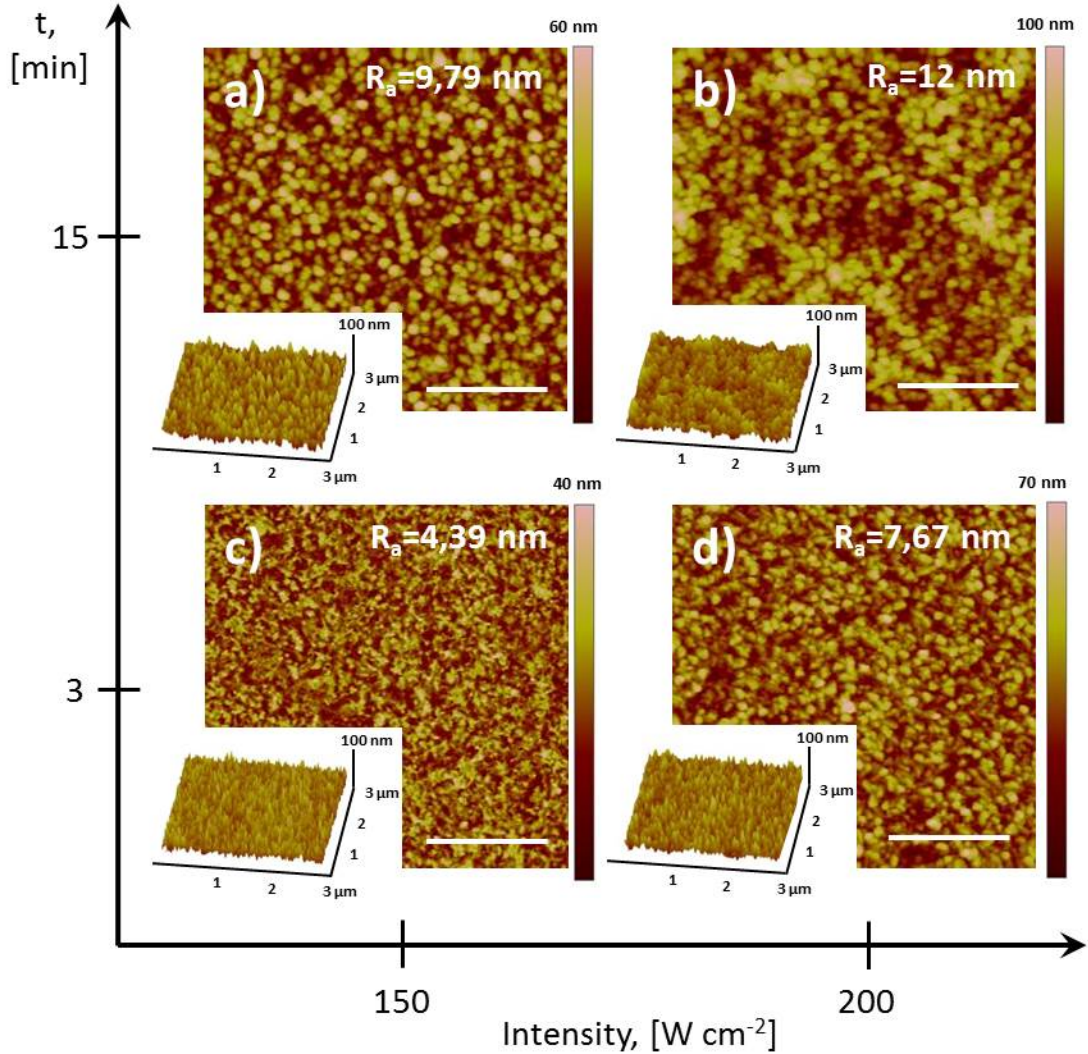
t,
[min]
15
3
a)
R_a=9,79 nm
60 nm
b)
R_a=12 nm
100 nm
c)
R_a=4,39 nm
40 nm
d)
R_a=7,67 nm
70 nm
100 nm
3 µm
2
1
1
2
3 µm
150
200
Intensity, [W cm^{-2}]

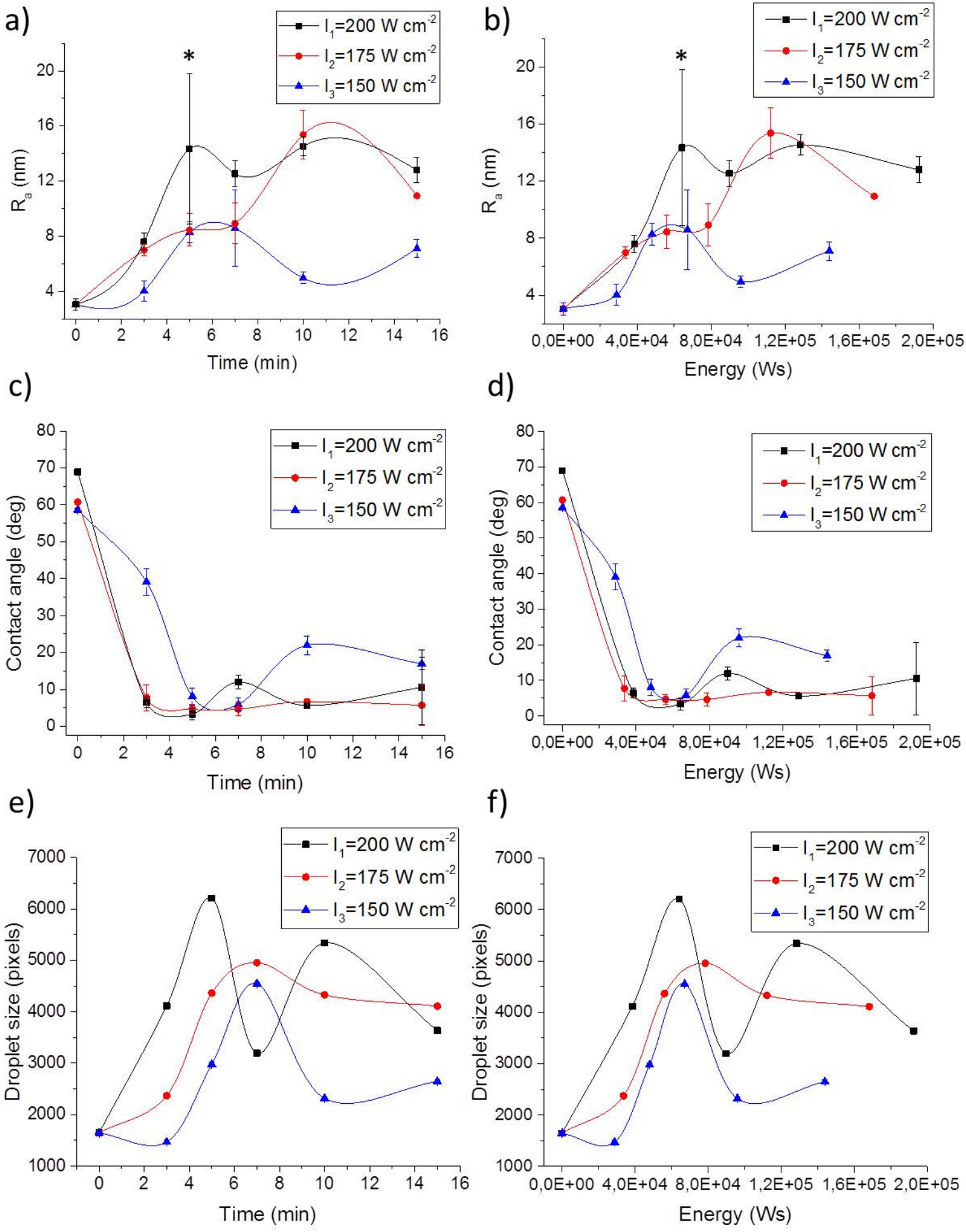
a)
b)
c)
d)
e)
f)
I_1=200 W cm^{-2}
I_2=175 W cm^{-2}
I_3=150 W cm^{-2}
R_a (nm)
Time (min)
Energy (Ws)
Contact angle (deg)
Droplet size (pixels)
*

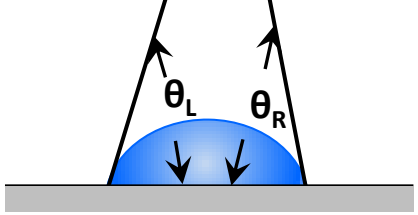
θL
θR

a)

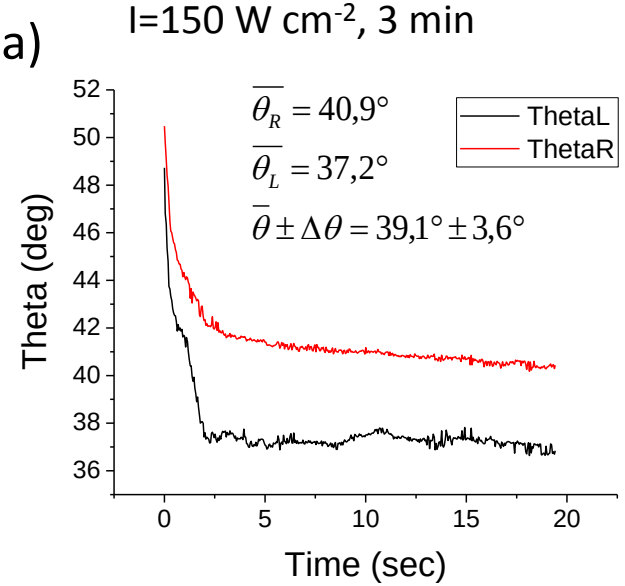
I=150 W cm-2, 3 min
$\overline{\theta_R} = 40{,}9°$
$\overline{\theta_L} = 37{,}2°$
$\overline{\theta} \pm \Delta\theta = 39{,}1° \pm 3{,}6°$
ThetaL
ThetaR
Theta (deg)
Time (sec)

b)

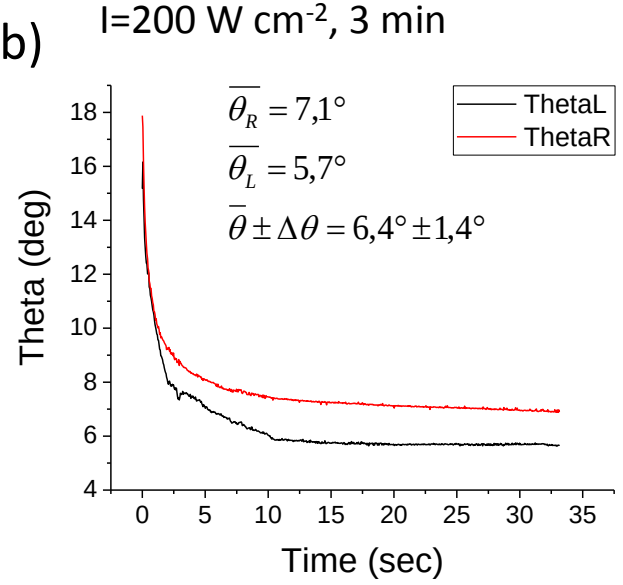
I=200 W cm-2, 3 min
$\overline{\theta_R} = 7{,}1°$
$\overline{\theta_L} = 5{,}7°$
$\overline{\theta} \pm \Delta\theta = 6{,}4° \pm 1{,}4°$
ThetaL
ThetaR
Theta (deg)
Time (sec)

c)

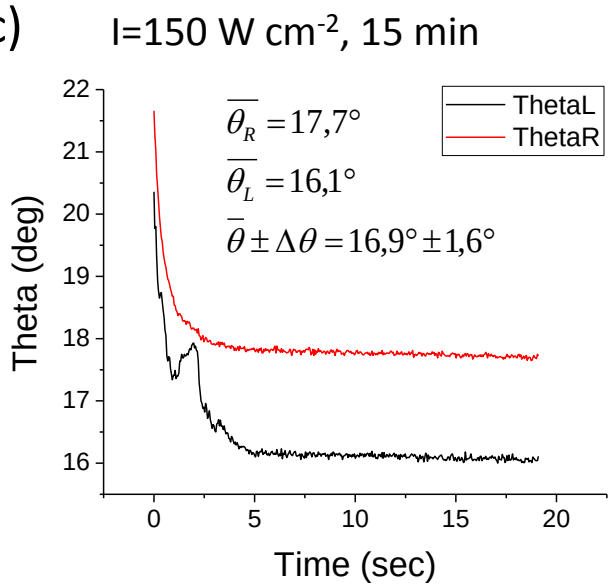
I=150 W cm-2, 15 min
$\overline{\theta_R} = 17{,}7°$
$\overline{\theta_L} = 16{,}1°$
$\overline{\theta} \pm \Delta\theta = 16{,}9° \pm 1{,}6°$
ThetaL
ThetaR
Theta (deg)
Time (sec)

d)

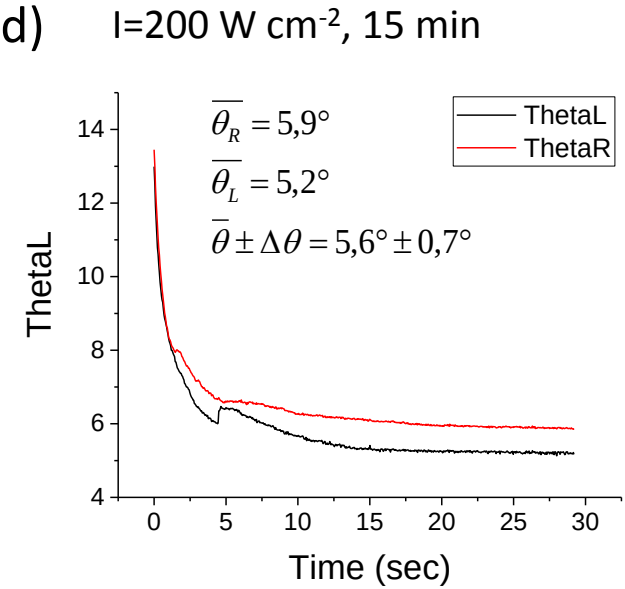
I=200 W cm-2, 15 min
$\overline{\theta_R} = 5{,}9°$
$\overline{\theta_L} = 5{,}2°$
$\overline{\theta} \pm \Delta\theta = 5{,}6° \pm 0{,}7°$
ThetaL
ThetaR
ThetaL
Time (sec)

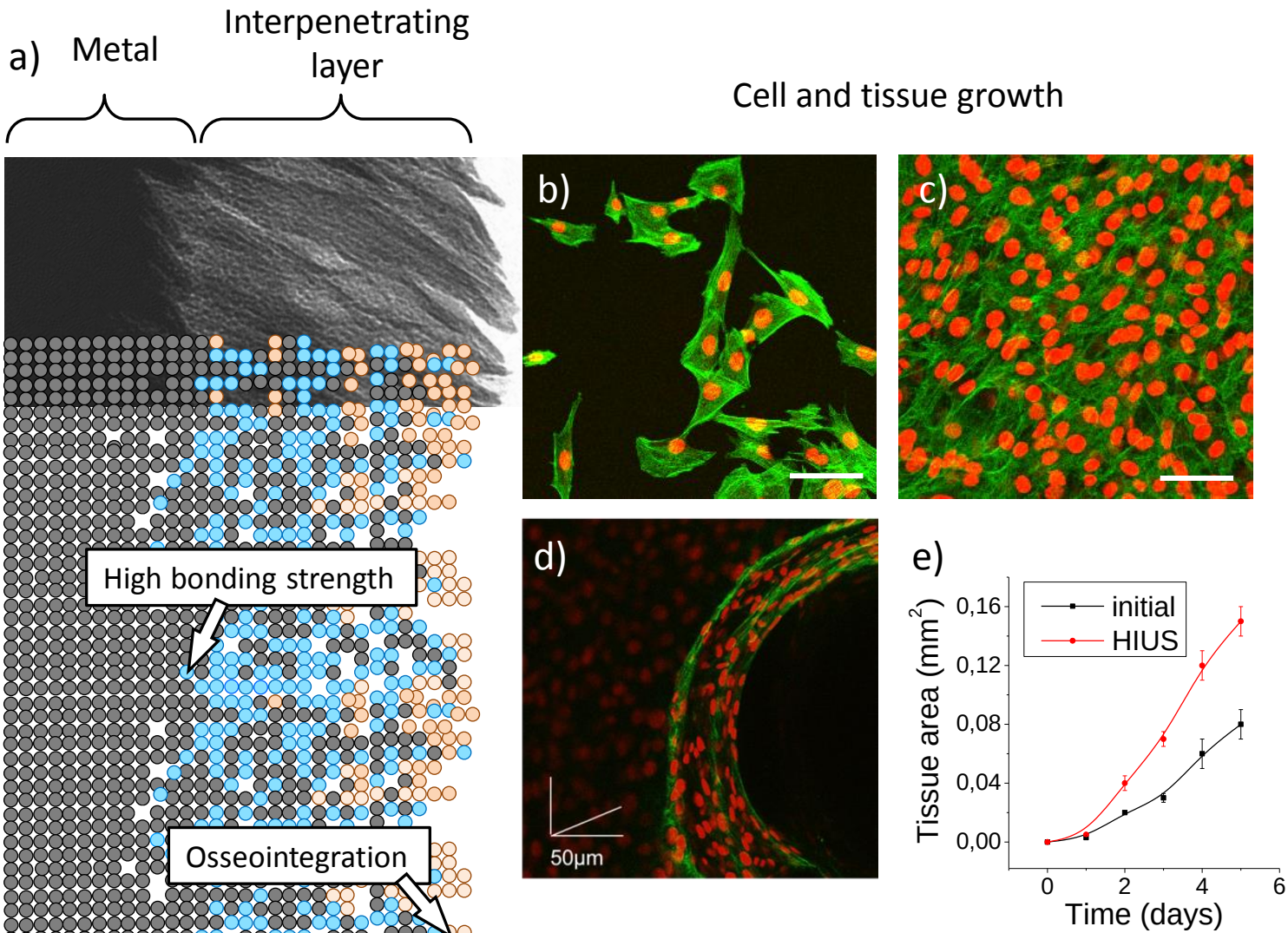
a)
Metal
Interpenetrating layer
High bonding strength
Osseointegration
Cell and tissue growth
b)
c)
d)
50µm
e)
initial
HIUS
Tissue area (mm²)
0,16
0,12
0,08
0,04
0,00
0
2
4
6
Time (days)

- Mesoporous titania surfaces were produced under high intensity ultrasound treatment
- Mesoporous titania surfaces show high wettability and surface roughness.
- Surface roughness and wettability can be tuned by changing ultrasonic parameters.
- Mesoropous titania surfaces show high biocompatibility with preosteoblast cell line.